Tunable Fe-vacancy disorder-order transition in FeSe thin films

Y. Fang,[1] D. H. Xie,[1] W. Zhang,[1] F. Chen,[2] W. Feng,[1] B. P. Xie,[2] D. L. Feng,[2] X. C. Lai,[1,*] and S. Y. Tan[1,†]

[1]*Science and Technology on Surface Physics and Chemistry Laboratory, Mianyang 621908, China*

[2]*Physics Department, Applied Surface Physics State Key Laboratory, and Advanced Materials Laboratory, Fudan University, Shanghai 200433, China*

(Received 20 November 2015; revised manuscript received 4 March 2016; published 10 May 2016)

Various Fe-vacancy orders have been reported in tetragonal β-$Fe_{1-x}Se$ single crystals and nanowires/nanosheets, which are similar to those found in alkali-metal intercalated $A_{1-x}Fe_{2-y}Se_2$ superconductors. Here we report the *in situ* angle-resolved photoemission spectroscopy study of Fe-vacancy disordered and ordered phases in FeSe multilayer thin films grown by molecular beam epitaxy. Low-temperature annealed FeSe films are identified to be Fe-vacancy disordered phase and electron doped. A further long-time low-temperature anneal can change the Fe-vacancy disordered phase to the ordered phase, which is found to be semiconductor/insulator with $\sqrt{5}\times\sqrt{5}$ superstructure and can be reversely changed to the disordered phase with a high-temperature anneal. Our results reveal that the disorder-order transition in FeSe thin films can be simply tuned by a vacuum anneal and the FeSe thin films provide rich information to understand the complex electronic structure and superconductivity of FeSe.

DOI: 10.1103/PhysRevB.93.184503

I. INTRODUCTION

High superconducting transition temperature (T_c) in FeSe and its intercalated compounds have attracted a great deal of attention in the area of condensed matter physics. β-$Fe_{1+\delta}Se$ has the simplest chemical and crystal structure with only superconducting FeSe layers in iron-based superconductors; it undergoes tetragonal to orthorhombic structural transition at $T_s \sim 90$ K and remarkable enhancement of T_c from ~8 to 36.7 K under pressure at 8.9 GPa [1–3]. Intercalating alkali-metal ions and small molecules in FeSe can also enhance T_c higher than 40 K [4–7]. Moreover, superconductivity in one unit cell (UC) FeSe thin films grown on $SrTiO_3$ (STO) substrate is particularly fascinating. A superconducting gap as large as 20 meV was identified by scanning tunneling spectroscopy (STS), and was later confirmed by angle-resolved photoemission spectroscopy (ARPES) measurements [8–11]. Then, the T_c above 40 and 100 K in 1-UC FeSe films was demonstrated by direct transport measurements [12] and *in situ* electrical transport measurements [13], respectively. FeSe and related compounds provide an ideal platform to study the mechanism of superconductivity in the iron-based superconductors.

In general, the parent compound which can be tuned to the superconductor by chemical doping or external pressure is of great importance to the investigation of the superconducting mechanism. The parent phase of the iron-pnictide superconductor is suggested to be metal with spin-density-wave (SDW) order. In the $A_{1-x}Fe_{2-y}Se_2$ superconductor, there exists an intrinsic mesoscopic phase separation of a superconducting phase and an Fe-vacancy ordered antiferromagnetic insulating phase [14–16]. The antiferromagnetic insulating phase $K_2Fe_4Se_5$ with $\sqrt{5}\times\sqrt{5}$ Fe-vacancy order is the most frequently observed Fe-vacancy order, and is suggested to be the parent compound owing to the close connection with the superconducting phase [17,18]. However, the phase separation makes it intricate to experimentally determine the intrinsic nature of the superconducting phase. A recent study on the nonsuperconducting Fe_4Se_5 [19], which exhibits the Fe-vacancy order and is magnetic, shows that it becomes superconducting after a high-temperature anneal, meanwhile the Fe-vacancy order disappears. This discovery suggests that the rich phases found in $A_{1-x}Fe_{2-y}Se_2$ are not exclusive in FeSe related superconductors, and the Fe-vacancy disorder and order have an intimate relationship with superconductivity. To better understand the superconducting mechanism in FeSe, the experimental study on the electronic structure of Fe-vacancy disordered and ordered phases becomes essential.

In this paper, we report the *in situ* angle-resolved photoemission spectroscopy study of Fe-vacancy disorder-order transition in FeSe multilayer thin films grown by molecular beam epitaxy (MBE). High-temperature (550 °C for 4 h) annealed multilayer FeSe thin films are found to be metallic with nematic order. Low-temperature (550 °C for 1 h and 250 °C for 3 h) annealed FeSe films are identified to be Fe-vacancy disordered phase with electron doping. A further long-time low-temperature (250 °C for 16 h) anneal can change the Fe-vacancy disordered phase to ordered phase, which is found to be semiconductor/insulator with $\sqrt{5}\times\sqrt{5}$ superstructure and can be reversely changed to disordered phase with a high-temperature anneal. Our results reveal that the disorder-order transition in FeSe thin films can be simply tuned by a vacuum anneal.

II. EXPERIMENT

High-quality FeSe single-crystalline thin films were grown on the TiO_2-terminated and Nb-doped $SrTiO_3$ (0.5 wt%) substrate with the molecular beam epitaxy (MBE) method following the previous reports [8,11]. The STO substrate was degassed at 550 °C for 3 h in vacuum, and then heated to 950 °C under the Se flux for 30 min. During growth, the substrate was kept at 450 °C with the Se flux 20 times greater than Fe by

*laixinchun@caep.cn

†sytan4444@163.com

codeposition. The properties of FeSe thin films can be tuned by varying the anneal temperature and length of the anneal time. The multilayer films annealed at 550 °C after growth in vacuum for 4 h have been proven to be stoichiometric FeSe with nematic order by both STM and ARPES results [8,11,20,21]. When the as-grown film was annealed at 550 °C for 1 h and 250 °C for 3 h, we got the low-temperature annealed FeSe thin film. If we further annealed the low-temperature annealed FeSe at 250 °C for 16 h, we got the long-time low-temperature annealed FeSe thin film. The $Fe_{1-x}Co_xSe$ ($x = 0.08$) thin film was induced by depositing cobalt atoms on the surface of the as-grown FeSe thin film and a subsequent 4 h of the 550 °C annealing process [22].

After growth and anneal, the film was directly transferred from the MBE chamber into the ARPES chamber with typical vacuum of 5×10^{-11} mbar. ARPES was conducted with 21.2 eV photons from a helium discharge lamp. A Scienta R4000 analyzer was used to record ARPES spectra with typical energy and angular resolutions of 10 meV and 0.2°, respectively. A freshly evaporated gold sample in electrical contact with the FeSe sample served to calibrate E_F.

III. RESULTS AND DISCUSSIONS

The as-grown multilayer FeSe thin films annealed at high temperature (550 °C for 4 h) have been demonstrated to have nematic order in the previous studies [11,21,22]. The Fermi surface topologies and band structures of high-temperature annealed FeSe films thicker than 2 UC are very much alike (named pristine FeSe hereafter). Taking 50-UC FeSe thin films as an example, the observed Fermi surface of pristine FeSe consists of crosslike electron pockets centered at M and elliptical hole pockets centered at Γ, as shown in Figs. 1(a1) and 1(b1). The 1-UC FeSe thin films have only circular electron pockets around M with typical 0.12 e^-/Fe [Figs. 1(a2) and 1(b2)], which are thought to be heavily doped by the electrons from the STO substrate. The cobalt-doped multilayer $Fe_{1-x}Co_xSe$ ($x = 0.08$) thin films also have circular electron pockets at M and some spectral weights at Γ with 0.08 e^-/Fe [Figs. 1(a3) and 1(b3)]. When the as-grown multilayer FeSe is annealed at 550 °C for 1 h and 250 °C for 3 h, the electronic structure changes dramatically. The Fermi surface of 40-UC low-temperature annealed FeSe (referred to as VD FeSe hereafter) consists of elliptical electron pockets centered

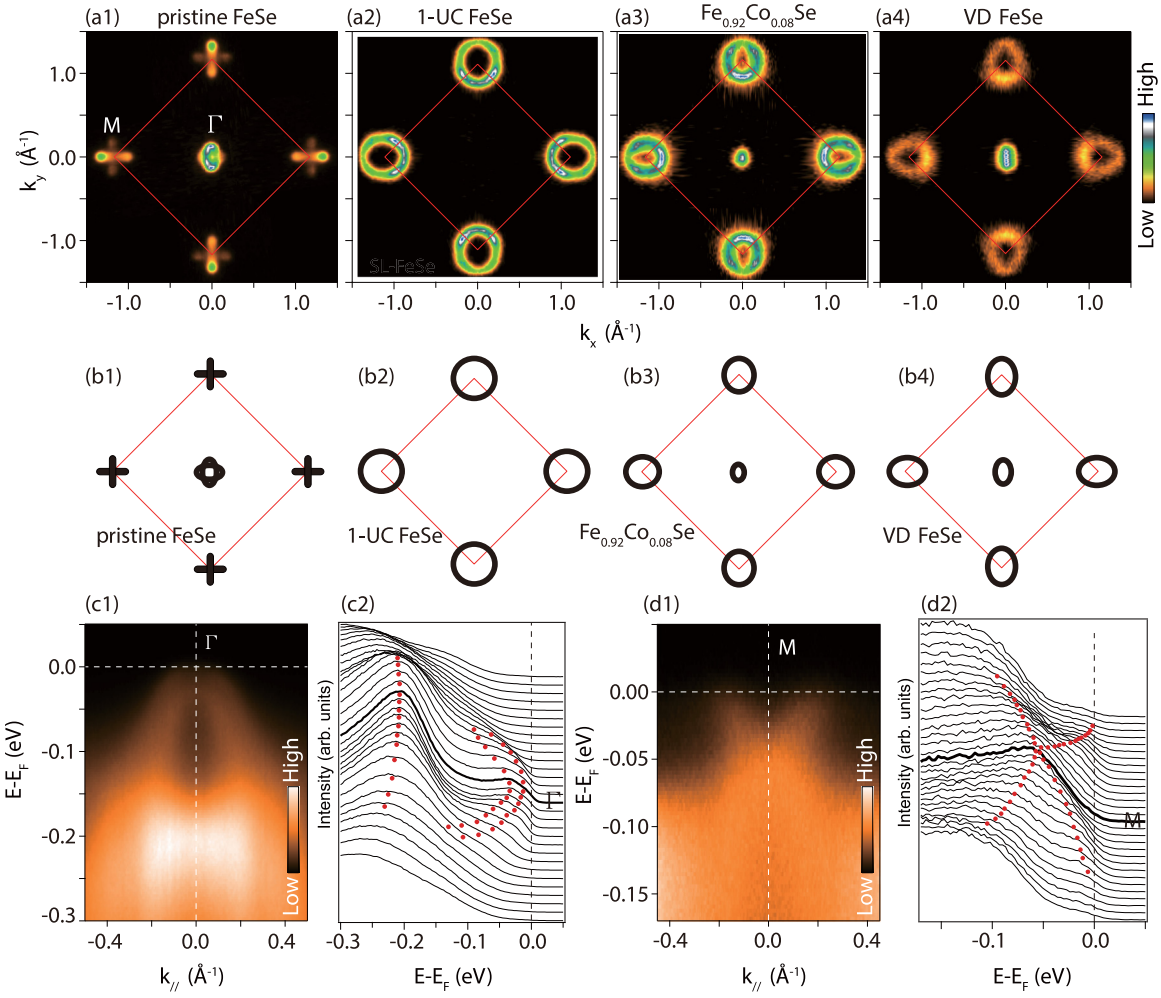

FIG. 1. Electronic structure of VD FeSe. (a1–a4) Fermi surface topologies of various FeSe thin films measured at 30 K integrated over a ($E_F - 10$ meV, $E_F + 10$ meV) window. (b1–b4) Schematic drawing of the Fermi surface topologies for various phases of FeSe thin films; the sizes of the Fermi pockets are extracted from (a) for clarity. (c1, c2) Photoemission intensity around Γ and the corresponding energy distribution curves (EDCs) of VD FeSe. (d1, d2) Photoemission intensity around M and the corresponding energy distribution curves of VD FeSe.

around M and some spectral weights at Γ, which is obviously electron doped with $0.06\,e^-$/Fe based on the calculated Luttinger volume [Figs. 1(a4) and 1(b4)]. The Fermi surface of VD FeSe is very similar to 1-UC FeSe and $Fe_{0.92}Co_{0.08}Se$, which are both heavily electron doped. The band structures of VD FeSe around Γ and M are shown in Figs. 1(c) and 1(d). Two holelike bands can be clearly resolved at Γ, whose band tops barely touch E_F and contribute to the spectral weights at the Brillouin zone center. At M, one electronlike band which forms the elliptical electron pocket and a holelike band located beneath the electron band can be resolved.

Obviously, the VD FeSe is a new phase whose electronic structure differs drastically from pristine FeSe. The low-energy electron diffraction (LEED) pattern of VD FeSe shows clearly tetragonal symmetry without any sign of superstructure [Fig. 3(d1)], which rules out the possibilities of structural transition or surface reconstruction. Compared with the epitaxial growth process of pristine FeSe, the only difference is that VD FeSe was annealed under lower temperature. Varying the anneal temperature and time would remarkably influence the stoichiometry of FeSe, which in turn changes the electronic structure of FeSe [23]. Different anneal temperatures are likely to result in a different Fe/Se ratio; that is to say, VD FeSe may be Se-rich $FeSe_{1+x}$ or Fe-rich $Fe_{1+x}Se$. The Se flux was kept 20 times greater than Fe by codeposition during growth; it is unlikely that excess Fe can survive under Se-rich conditions. According to the *in situ* STM measurements [20,24], the as-grown FeSe thin films have extra Se on the surface due to the Se-rich growth condition. Annealing the as-grown films at an elevated temperature (typically 550 °C in our study) will remove the extra Se to form stoichiometric FeSe (pristine FeSe). Compared with pristine FeSe, the VD FeSe films were annealed at a much lower temperature (250 °C), which cannot remove the extra Se completely and leave a Se-rich surface. Therefore, it is natural to conclude that VD FeSe is Se-rich $FeSe_{1+x}$ (excess Se or Fe vacancies) rather than Fe-rich $Fe_{1+x}Se$ (excess Fe or Se vacancies).

For the Se-rich $FeSe_{1+x}$, excess Se adatoms or Fe vacancies are two alternative explanations. According to the *in situ* STM measurements [20,24], FeSe films with extra Se adatoms show typical semiconducting behavior with a gap of ∼0.6 eV. Furthermore, Shanavas *et al.* [25] theoretically predicted that excess Se on FeSe will shrink the electron pockets and induce a pseudogap just above the Fermi level. The VD FeSe in our study shows clearly metallic behavior, which conflicts with the excess Se situation, leaving Fe vacancies the only possibility. Generally speaking, it is often expected that Se vacancies should result in electron doping and Fe vacancies should result in hole doping. Unexpectedly, Berlijn *et al.* [26] studied the doping effects of Se vacancies in monolayer FeSe and found that in terms of the Fe 3d bands, Se vacancies behave like hole dopants rather than electron dopants. Zhuang *et al.* [27] studied the effects of iron deficiencies in $Fe_xSe_{0.5}Te_{0.5}$ thin films on superconductivity and electronic properties. They found that the presence of Fe vacancies alters the charge carrier population by introducing electron charge carriers, with the Fe-deficient film showing more metallic behavior than the defect-free film. Furthermore, a theoretical study [28] on $K_{1-x}Fe_{2-y}Se_2$ found that the Fe-vacancy disorder raises the chemical potential significantly, eliminating the hole pockets around Γ and enlarging the electron pockets at M. According to the above analyses, we concluded that the low-temperature annealed VD FeSe stands for Fe-vacancy disordered FeSe. The Fe-vacancy disorder behaves like electron dopants to FeSe, which causes VD FeSe to appear electron doped compared with stoichiometric pristine FeSe.

To better understand the electronic structure of the electron-doped VD FeSe, we present the low-energy band structures of pristine FeSe, 1-UC FeSe, $Fe_{0.92}Co_{0.08}Se$, and VD FeSe around Γ and M in Fig. 2 for comparison. The pristine FeSe is charge neutral and all the other three are electron doped with different doping levels. From Fig. 2(b1) we can see that the two holelike bands which cross E_F and the relatively flat band ω located at about –190 meV at Γ in pristine FeSe both move downwards to high binding energy upon electron doping. The larger the doping level is, the higher binding energy the bands move to. While there is only a subtle difference between $Fe_{0.92}Co_{0.08}Se$ and VD FeSe at Γ, two holelike bands get totally reconstructed to one in 1-UC FeSe due to the interface effect. The obvious difference between the two electron-doped FeSe phases without interface effect is that the effective masses of the hole bands are much smaller in $Fe_{0.92}Co_{0.08}Se$ than in VD FeSe, which indicates weaker correlation strength in $Fe_{0.92}Co_{0.08}Se$ due to cobalt dosing.

The complicated band structure at M in pristine FeSe changes significantly with electron doping, as shown in Figs. 2(c) and 2(d). Two electronlike bands and two holelike bands exist at M in nematic ordered pristine FeSe, and the electron doping will suppress the nematic order and change the band structure topology. The electronic structures of $Fe_{0.92}Co_{0.08}Se$ and VD FeSe seem much alike, mainly consisting of an electron band which crosses E_F and a hole band located beneath. The bottoms of the electron bands are located at –70 and –50 meV in $Fe_{0.92}Co_{0.08}Se$ and VD FeSe, respectively, and again the effective mass of the electron band in $Fe_{0.92}Co_{0.08}Se$ is much smaller due to cobalt dosing. A gap of 60 meV opens between the intersectant electron and hole bands in 1-UC FeSe due to interface effect, as shown in Fig. 2(d2). The electronic structure of 1-UC FeSe is much different from the other two electron-doped ones [Fig. 2(e)], which indicates that the unique electronic structure of 1-UC FeSe is not originated from simply doping with electron carriers, and the FeSe/STO interface plays an important role in the determination of the unique electronic structure.

When the VD FeSe was further annealed at 250 °C for 16 h, we got the long-time low-temperature annealed FeSe (referred to as VO FeSe hereafter), which turns out to be a semiconductor/insulator judging by the photoemission data. The photoemission intensity maps of VO FeSe are shown in Fig. 3(a), which are integrated over a ($E_F - 20$ meV, $E_F +$ 20 meV) window. As shown in Fig. 3(a1), there is no obvious spectral weight at E_F, indicating its semiconducting/insulating nature. With decreasing binding energy, the spectral weight gets stronger and a clear constant energy dispersion contour emerges at $E_F - 200$ meV [Fig. 3(a4)]. Large spectral weight and a rectangular-shaped pocket appear around the Brillouin zone center, as shown in Figs. 3(a4) and 3(a5). The Brillouin zone size of VO FeSe determined from the high-symmetry points of the photoemission map is much smaller than VD FeSe. The value of the lattice constant derived from the

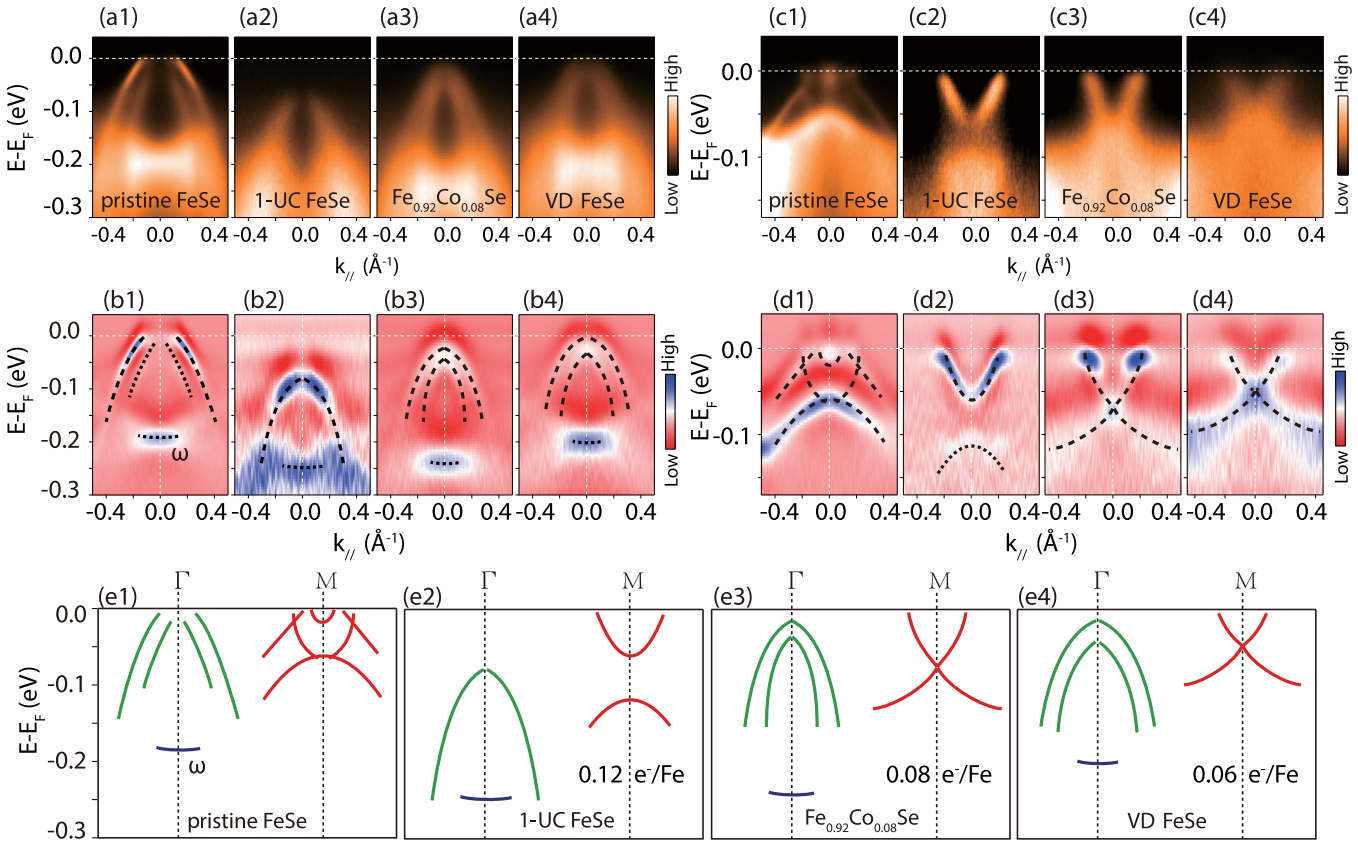

FIG. 2. Band structures of various phases of FeSe thin films. (a, b) The photoemission intensity (a1–a4) and its corresponding second derivative of the intensity plot (b1–b4) around Γ for pristine FeSe, 1-UC FeSe, $Fe_{0.92}Co_{0.08}Se$, and VD FeSe, respectively. (c, d) The photoemission intensity (c1–c4) and its corresponding second derivative of the intensity plot (d1–d4) around *M* for pristine FeSe, 1-UC FeSe, $Fe_{0.92}Co_{0.08}Se$, and VD FeSe, respectively. The dashed lines in (b, d) are guides to the eye. (e1–e4) Schematic band structures of pristine FeSe, 1-UC FeSe, $Fe_{0.92}Co_{0.08}Se$, and VD FeSe, respectively. The doping levels are calculated based on the Luttinger volume.

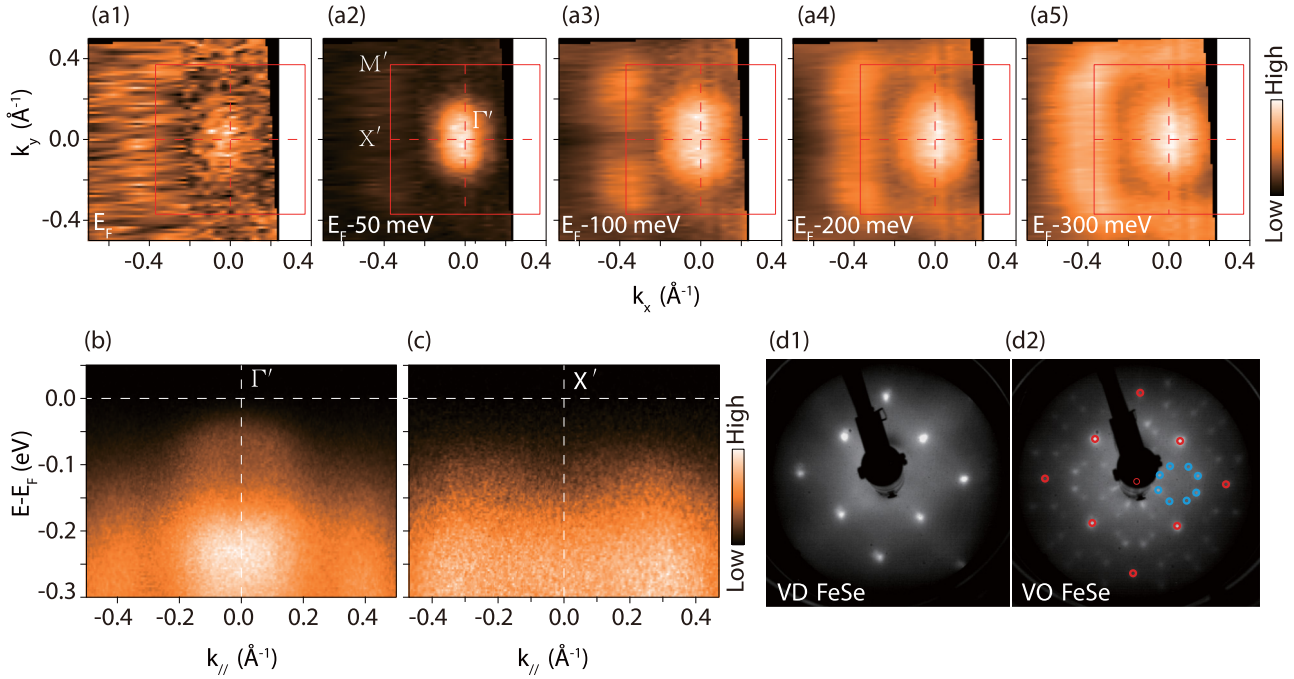

FIG. 3. Electronic structure of VO FeSe. (a1–a5) Constant-energy maps at different binding energies from E_F to $E_F - 300$ meV for VO FeSe. (b, c) The photoemission intensity of VO FeSe around Γ′ and *X*′, respectively. (d) The LEED patterns of VD FeSe (d1) and VO FeSe (d2).

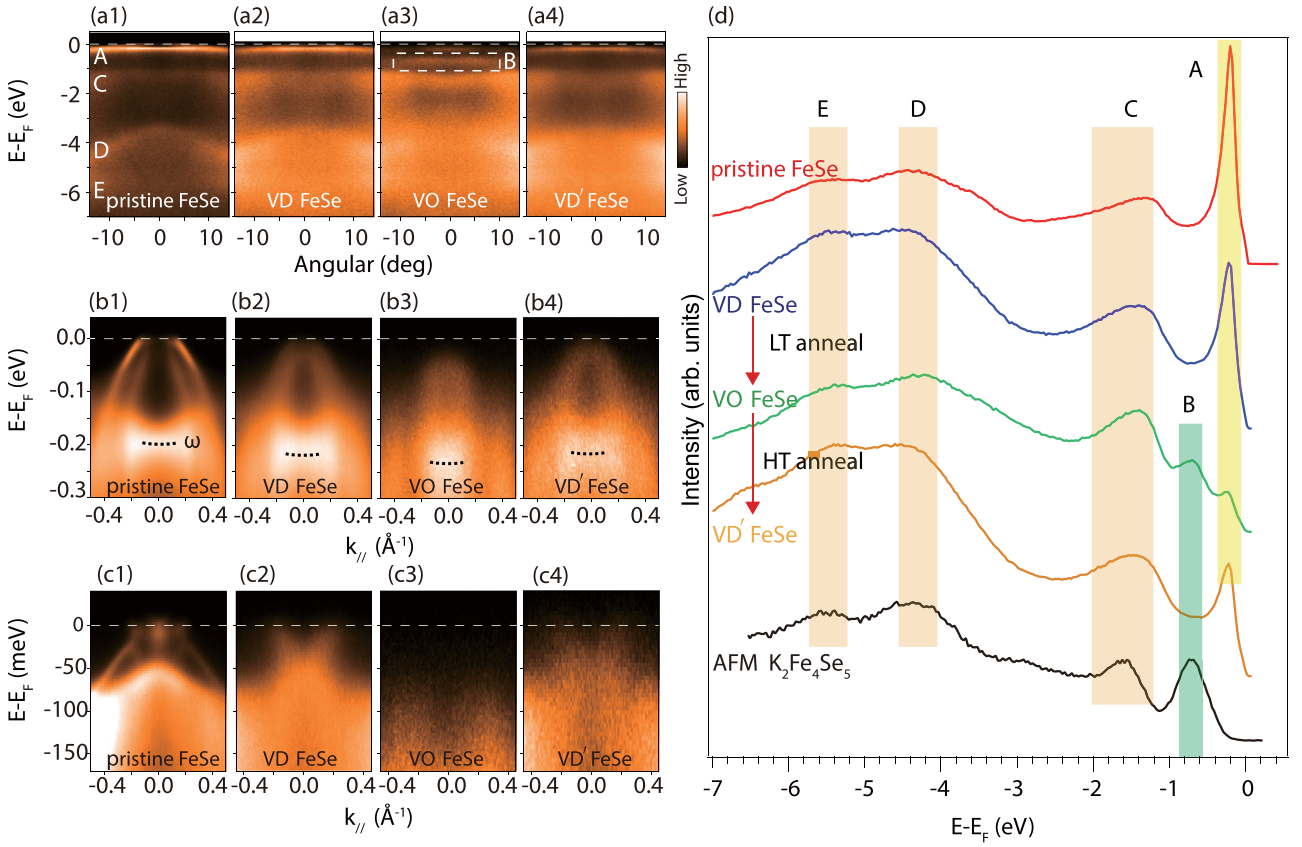

FIG. 4. Fe-vacancy disorder-order transition in FeSe thin films. (a1–a4) Valence-band structure at Γ for pristine FeSe, VD FeSe, VO FeSe, and VD′ FeSe, respectively. (b1–b4) Low-energy band structure at Γ for pristine FeSe, VD FeSe, VO FeSe, and VD′ FeSe, respectively. (c1–c4) Low-energy band structure at M for pristine FeSe, VD FeSe, VO FeSe, and VD′ FeSe, respectively. (d) Valence-band photoemission spectra at Γ point for pristine FeSe, VD FeSe, VO FeSe, VD′ FeSe, and $K_2Fe_4Se_5$, respectively.

reciprocal of the Brillouin zone size is about $a = b = 8.5$ Å in VO FeSe, which is $\sqrt{5}$ times that in VD FeSe ($a = b = 3.8$ Å).

The LEED patterns of VD FeSe and VO FeSe are shown in Fig. 3(d). The LEED pattern of VD FeSe shows typical tetragonal symmetry without any sign of superstructure [Fig. 3(d1)]. Compared with the LEED pattern of VD FeSe, we can see clear $\sqrt{5}\times\sqrt{5}$ superstructure in that of VO FeSe [Fig. 3(d2)]. The eight blue dots form a circular ring in between each four red dots, which is clear evidence that $\sqrt{5}\times\sqrt{5}$ superstructures emerge on the surface. The band structures at the reconstructed high-symmetry points Γ′ and X' of VO FeSe are shown in Figs. 3(b) and 3(c). The density of states near E_F are significantly suppressed at Γ′ and X' in VO FeSe, which shows typical semiconducting/insulating behavior. Judging from the ARPES results and the LEED patterns, we can conclude that the VO FeSe stands for Fe-vacancy ordered FeSe, which is a semiconductor/insulator. Long-time low-temperature annealing changes the disordered Fe vacancies to an ordered state, leading to the $\sqrt{5}\times\sqrt{5}$ LEED pattern and the reconstructed band structures of VO FeSe.

As mentioned above, the VD FeSe changes to $\sqrt{5}\times\sqrt{5}$ ordered VO FeSe under a 250 °C vacuum anneal for 16 h. Interestingly, if we anneal the VO FeSe at 550 °C high temperature for 2 h, the $\sqrt{5}\times\sqrt{5}$ superstructure will disappear and the film changes to the Fe-vacancy disordered phase again (referred to as VD′ FeSe). The valence-band and low-energy-band structure for pristine FeSe, VD FeSe, VO FeSe, and VD′ FeSe are present in Fig. 4. If we ignore the influence of sample quality on the band structure, the VD FeSe and VD′ FeSe have almost the same characteristic band structures, as shown in Figs. 4(a2) and 4(a4), 4(b2) and 4(b4), and 4(c2) and 4(c4), which indicates that they are indeed the same phase. That is to say, the VO FeSe can be reversely tuned to VD FeSe through a 550 °C high-temperature anneal.

Although the low-energy band structures have much difference between pristine FeSe, VD FeSe, and VO FeSe [Figs. 4(b) and 4(c)], their valence bands are relatively similar [Fig. 4(a)]. We plot the angle-integrated spectra around Γ for pristine FeSe, VD FeSe, VO FeSe, VD′ FeSe, and $K_2Fe_4Se_5$ together in Fig. 4(d). There are four main features in the valence bands of FeSe thin films, which locate at about –0.2, –1.3, –4.4, and –5.5 eV and are named A, C, D, and E, respectively. The C, D, and E peaks can be seen in all the FeSe thin films and $K_2Fe_4Se_5$ single crystals, which may correspond to the characteristic features of FeSe related compounds. A special band (band B) appears only in VO FeSe [Fig. 4(a3)], which lies at about –700 meV below E_F [Fig. 4(d)] and has been proven to be the characteristic feature of $K_2Fe_4Se_5$ [15]. $K_2Fe_4Se_5$ is an antiferromagnetic (AFM) insulating phase with Fe-vacancy $\sqrt{5}\times\sqrt{5}$ order, which is suggested to be the parent compound owing to the close connection with

the superconducting phase [17,18]. Therefore, we are more convinced that the VO FeSe corresponds to the Fe-vacancy ordered phase similarly to $K_2Fe_4Se_5$. Based on our ARPES and LEED data, we can conclude that low-temperature annealed FeSe thin films (VD FeSe) are Fe-vacancy disordered $Fe_{1-x}Se$; further low-temperature annealed FeSe thin films (VO FeSe) are $\sqrt{5}\times\sqrt{5}$ Fe-vacancy ordered phase and the disorder-order transition can be simply tuned by a vacuum anneal.

IV. DISCUSSION AND CONCLUSION

Identifying the parent compound and understanding its doping evolution is a crucial step in elucidating the superconducting pairing mechanism. For the potassium-intercalated FeSe compounds, there has been significant debate regarding what the parent compound is [29–32]. A recent study [33] shows that the Fe-vacancy ordered $K_2Fe_4Se_5$ is the magnetic, Mott insulating parent compound of the superconducting state. Insulating $K_2Fe_4Se_5$ becomes a superconductor after high-temperature annealing, and the overall picture indicates that superconductivity in $K_{2-x}Fe_{4+y}Se_5$ originates from the Fe-vacancy order-to-disorder transition. Nonsuperconducting FeTe with bicollinear antiferromagnetic order is always considered as the parent compound of FeSe [34,35]. However, a recent transmission electron microscope (TEM) study [19] on the nonsuperconducting Fe_4Se_5, which exhibits the $\sqrt{5}\times\sqrt{5}$ Fe-vacancy order and is magnetic, shows that it becomes superconducting after high-temperature annealing; meanwhile the Fe-vacancy order disappears.

Our LEED and ARPES results on the MBE-grown FeSe thin films show that the $\sqrt{5}\times\sqrt{5}$ Fe-vacancy ordered VO FeSe is a semiconductor/insulator and can be tuned to Fe-vacancy disordered VD FeSe with electron doping. The Fe-vacancy order-disorder transition in FeSe films is similar to that found in $K_{2-x}Fe_{4+y}Se_5$ and Fe_4Se_5 single crystals [19,33]. Furthermore, the Fe-vacancy order-disorder transition in FeSe films resembles the typical phase diagram of cuprates, where doping-induced insulator-superconductor transitions are widely observed. The key issue is whether the VD FeSe is superconducting or not. It was found recently [36] that Fe-vacancy disordered FeSe thin films fabricated by pulsed-laser deposition (PLD) are superconducting with the highest T_c up to 15.2 K. The VD FeSe grown by MBE in our study is also likely superconducting; its *Tc* is too low to be detected by our ARPES instrument with the lowest detecting temperature of 30 K. Further low-temperature STM (down to 4 K) studies are currently in progress to identify the superconductivity of the VD FeSe.

In summary, we report the *in situ* angle-resolved photoemission spectroscopy study of Fe-vacancy disorder-order transition in FeSe multilayer thin films grown by molecular beam epitaxy. Low-temperature annealed FeSe films are identified to be Fe-vacancy disordered phase and electron doped. A further long-time low-temperature anneal can change the Fe-vacancy disordered phase to the ordered phase, which is found to be semiconductor/insulator with $\sqrt{5}\times\sqrt{5}$ superstructure and can be reversely changed to the disordered phase with a high-temperature anneal. Our results reveal that the disorder-order transition in FeSe thin films can be simply tuned by a vacuum anneal and the FeSe thin films with precisely controllable crystal structure, stoichiometry, and thickness can provide rich information to understand the complex electronic structure and superconductivity of FeSe.

ACKNOWLEDGMENTS

We gratefully acknowledge helpful discussions with Dr. X. H. Niu. This work is supported by the Foundation of President of China Academy of Engineering Physics (Grant No. 201501037) and by the National Natural Science Foundation of China (Grant No. 11504341).

[1] F. C. Hsu, J. Y. Luo, K. W. Yeh, T. K. Chen, T. W. Huang, P. M. Wu, Y. C. Lee, Y. L. Huang, Y. Y. Chu, D. C. Yan, and M. K. Wu, Proc. Natl. Acad. Sci. USA **105**, 14262 (2008).

[2] Y. Mizuguchi, F. Tomioka, S. Tsuda, T. Yamaguchi, and Y. Takano, Appl. Phys. Lett. **93**, 152505 (2008).

[3] S. Medvedev, T. M. McQueen, A. Troyan, T. Palasyuk, M. I. Eremets, R. J. Cava, S. Naghavi, F. Casper, V. Ksenofontov, G. Wortmann, and C. Felser, Nat. Mater. **8**, 630 (2009).

[4] J. Guo, S. Jin, G. Wang, S. Wang, K. Zhu, T. Zhou, M. He, and X. Chen, Phys. Rev. B **82**, 180520 (2010).

[5] M.-H. Fang, H.-D. Wang, C.-H. Dong, Z.-J. Li, C.-M. Feng, J. Chen, and H. Q. Yuan, Europhys. Lett. **94**, 27009 (2011).

[6] M. Burrard-Lucas, D. G. Free, S. J. Sedlmaier, J. D. Wright, S. J. Cassidy, Y. Hara, A. J. Corkett, T. Lancaster, P. J. Baker, S. J. Blundell, and S. J. Clarke, Nat. Mater. **12**, 15 (2012).

[7] X. F. Lu, N. Z. Wang, H. Wu, Y. P. Wu, D. Zhao, X. Z. Zeng, X. G. Luo, T. Wu, W. Bao, G. H. Zhang, F. Q. Huang, Q. Z. Huang, and X. H. Chen, Nat. Mater. **14**, 325 (2014).

[8] Q.-Y. Wang, Z. Li, W.-H. Zhang, Z.-C. Zhang, J.-S. Zhang, W. Li, H. Ding, Y.-B. Ou, P. Deng, K. Chang, J. Wen, C.-L. Song, K. He, J.-F. Jia, S.-H. Ji, Y.-Y. Wang, L.-L. Wang, X. Chen, X.-C. Ma, and Q.-K. Xue, Chin. Phys. Lett. **29**, 037402 (2012).

[9] D. Liu, W. Zhang, D. Mou, J. He, Y. B. Ou, Q. Y. Wang, Z. Li, L. Wang, L. Zhao, S. He, Y. Peng, X. Liu, C. Chen, L. Yu, G. Liu, X. Dong, J. Zhang, C. Chen, Z. Xu, J. Hu *et al.*, Nat. Commun. **3**, 931 (2012).

[10] S. He, J. He, W. Zhang, L. Zhao, D. Liu, X. Liu, D. Mou, Y.-B. Ou, Q.-Y. Wang, Z. Li, L. Wang, Y. Peng, Y. Liu, C. Chen, L. Yu, G. Liu, X. Dong, J. Zhang, C. Chen, Z. Xu *et al.*, Nat. Mater. **12**, 605 (2013).

[11] S. Y. Tan, Y. Zhang, M. Xia, Z. R. Ye, F. Chen, X. Xie, R. Peng, D. F. Xu, Q. Fan, H. C. Xu, J. Juan, T. Zhang, X. C. Lai, T. Xiang, J. P. Hu, B. P. Xie, and D. L. Feng, Nat. Mater. **12**, 634 (2013).

[12] W. Zhang, Y. Sun, J. Zhang, F. Li, M. Guo, Y. Zhao, H. Zhang, J. Peng, Y. Xing, H. Wang, T. Fujita, A. Hirata, Z. Li, H. Ding,

C. Tang, M. Wang, Q. Wang, K. He, S. Ji, X. Chen *et al.*, Chin. Phys. Lett. **31**, 017401 (2013).
[13] J. F. Ge, Z. L. Liu, C. Liu, C. L. Gao, D. Qian, Q. K. Xue, Y. Liu, and J. F. Jia, Nat. Mater. **14**, 285 (2014).
[14] Z. Wang, Y. J. Song, H. L. Shi, Z. W. Wang, Z. Chen, H. F. Tian, G. F. Chen, J. G. Guo, H. X. Yang, and J. Q. Li, Phys. Rev. B **83**, 140505 (2011).
[15] F. Chen, M. Xu, Q. Q. Ge, Y. Zhang, Z. R. Ye, L. X. Yang, J. Jiang, B. P. Xie, R. C. Che, M. Zhang, A. F. Wang, X. H. Chen, D. W. Shen, J. P. Hu, and D. L. Feng, Phys. Rev. X **1**, 021020 (2011).
[16] W. Li, H. Ding, P. Deng, K. Chang, C. Song, K. He, L. Wang, X. Ma, J.-P. Hu, X. Chen, and Q.-K. Xue, Nat. Phys. **8**, 126 (2011).
[17] X.-W. Yan, M. Gao, Z.-Y. Lu, and T. Xiang, Phys. Rev. B **83**, 233205 (2011).
[18] W. Bao, Q.-Z. Huang, G.-F. Chen, D.-M. Wang, J.-B. He, and Y.-M. Qiu, Chin. Phys. Lett. **28**, 086104 (2011).
[19] T. K. Chen, C. C. Chang, H. H. Chang, A. H. Fang, C. H. Wang, W. H. Chao, C. M. Tseng, Y. C. Lee, Y. R. Wu, M. H. Wen, H. Y. Tang, F. R. Chen, M. J. Wang, M. K. Wu, and D. Van Dyck, Proc. Natl. Acad. Sci. USA **111**, 63 (2014).
[20] C.-L. Song, Y.-L. Wang, Y.-P. Jiang, Z. Li, L. Wang, K. He, X. Chen, X.-C. Ma, and Q.-K. Xue, Phys. Rev. B **84**, 020503 (2011).
[21] Y. Zhang, M. Yi, Z.-K. Liu, W. Li, J. J. Lee, R. G. Moore, M. Hashimoto, N. Masamichi, H. Eisaki, S.-K. Mo, Z. Hussain, T. P. Devereaux, Z.-X. Shen, and D. H. Lu, arXiv:1503.01556 (2015).
[22] S. Y. Tan, Y. Fang, D. H. Xie, W. Feng, C. H. P. Wen, Q. Song, Q. Y. Chen, W. Zhang, Y. Zhang, L. Z. Luo, B. P. Xie, X. C. Lai, and D. L. Feng, Phys. Rev. B **93**, 104513 (2016).
[23] T. M. McQueen, Q. Huang, V. Ksenofontov, C. Felser, Q. Xu, H. Zandbergen, Y. S. Hor, J. Allred, A. J. Williams, D. Qu, J. Checkelsky, N. P. Ong, and R. J. Cava, Phys. Rev. B **79**, 014522 (2009).
[24] Z. Li, J. P. Peng, H. M. Zhang, W. H. Zhang, H. Ding, P. Deng, K. Chang, C. L. Song, S. H. Ji, L. Wang, K. He, X. Chen, Q. K. Xue, and X. C. Ma, J. Phys.: Condens. Matter **26**, 265002 (2014).
[25] K. V. Shanavas and D. J. Singh, Phys. Rev. B **92**, 035144 (2015).
[26] T. Berlijn, H.-P. Cheng, P. J. Hirschfeld, and W. Ku, Phys. Rev. B **89**, 020501 (2014).
[27] J. C. Zhuang, W. K. Yeoh, X. Y. Cui, J. H. Kim, D. Q. Shi, Z. X. Shi, S. P. Ringer, X. L. Wang, and S. X. Dou, Appl. Phys. Lett. **104**, 262601 (2014).
[28] T. Berlijn, P. J. Hirschfeld, and W. Ku, Phys. Rev. Lett. **109**, 147003 (2012).
[29] W. Li, H. Ding, Z. Li, P. Deng, K. Chang, K. He, S. Ji, L. Wang, X. Ma, J.-P. Hu, X. Chen, and Q.-K. Xue, Phys. Rev. Lett. **109**, 057003 (2012).
[30] X. Ding, D. Fang, Z. Wang, H. Yang, J. Liu, Q. Deng, G. Ma, C. Meng, Y. Hu, and H. H. Wen, Nat. Commun. **4**, 1897 (2013).
[31] J. Zhao, H. Cao, E. Bourret-Courchesne, D. H. Lee, and R. J. Birgeneau, Phys. Rev. Lett. **109**, 267003 (2012).
[32] C. Cao and F. Zhang, Phys. Rev. B **87**, 161105 (2013).
[33] C.-H. Wang, T.-K. Chen, C.-C. Chang, C.-H. Hsu, Y.-C. Lee, M.-J. Wang, P. M. Wu, and M.-K. Wu, Europhys. Lett. **111**, 27004 (2015).
[34] K.-W. Yeh, T.-W. Huang, Y.-l. Huang, T.-K. Chen, F.-C. Hsu, P. M. Wu, Y.-C. Lee, Y.-Y. Chu, C.-L. Chen, J.-Y. Luo, D.-C. Yan, and M.-K. Wu, Europhys. Lett. **84**, 37002 (2008).
[35] W. Bao, Y. Qiu, Q. Huang, M. A. Green, P. Zajdel, M. R. Fitzsimmons, M. Zhernenkov, S. Chang, M. Fang, B. Qian, E. K. Vehstedt, J. Yang, H. M. Pham, L. Spinu, and Z. Q. Mao, Phys. Rev. Lett. **102**, 247001 (2009).
[36] W. Qiu, Z. Ma, Y. Liu, X. Wang, and S. X. Dou, arXiv:1512.00352 (2015).